Physics and Chemistry of Minerals (2019) 46:717–725
https://doi.org/10.1007/s00269-019-01033-1

ORIGINAL PAPER

Structural behavior of a stuffed derivative of α-quartz, $Mg_{0.5}AlSiO_4$, at high temperature: an in situ synchrotron XRD study

Hongwu Xu[1] · Xujie Lü[1] · Peter J. Heaney[2] · Yang Ren[3]

Received: 24 February 2019 / Accepted: 1 April 2019 / Published online: 11 April 2019

Abstract
High-temperature structural behavior of a stuffed derivative of α-quartz, $Mg_{0.5}AlSiO_4$, has been investigated using in situ synchrotron-based angle-dispersive powder X-ray diffraction (XRD) from 299 to 1273 K. Rietveld analysis of the XRD data indicates that the framework of $Mg_{0.5}AlSiO_4$ remains isostructural with α-quartz throughout the temperature range tested. As in α-quartz, unit-cell parameters *a* and *c* and cell volume *V* of $Mg_{0.5}AlSiO_4$ increase with increasing temperature, primarily due to progressive tilting of [(Al,Si)O_4] tetrahedra along the *a* axes. However, the rates of increase in the cell parameters and the rate of decrease in the tetrahedral tilt angle (δ) are much smaller for $Mg_{0.5}AlSiO_4$ than for α-quartz. This behavior can be attributed to the occupancy of Mg^{2+} over the octahedral channel sites in the α-quartz-type framework, effectively hindering the [(Al,Si)O_4] tetrahedral tilting. As a result, the α- to β-quartz phase transformation, which exists in silica at 846 K, does not occur in $Mg_{0.5}AlSiO_4$ up to 1273 K, and probably beyond, to its melting point.

Keywords α-Quartz · Stuffed derivative · Crystal structure · High temperature · Thermal expansion · Synchrotron X-ray diffraction · Rietveld analysis

Introduction

Although natural quartz is intolerant of ionic substitutions (mostly at the levels of hundreds of ppm) (Keith and Tuttle 1952; Ghiorso et al. 1979; Smith and Steele 1984), replacement of Si^{4+} cations by the larger Al^{3+} can facilitate incorporation of several small cations, including Li^+, Mg^{2+}, Zn^{2+}, H^+ and Na^+, into the quartz framework (Schulz 1971; Schulz et al. 1971a, b; Tscherry et al. 1972; Guth and Heger 1979; Müller et al. 1988, 1990; Paulus et al. 1990; Sternitzke and Müller 1991; Palmer 1994; Xu et al. 1999a, b, c, 2000a, 2001a; Heaney 2000; Phillips et al. 2000). The charge-coupled substitution, $Si^{4+} \rightarrow Al^{3+} + M^+$ or ½ M^{2+} ($M^+ = Li^+$, H^+, Na^+; $M^{2+} = Mg^{2+}$, Zn^{2+}), produces a series of phases that Buerger (1954) classified as "stuffed derivatives of quartz".

Depending on the size and concentration of substituting cations, stuffed derivatives of quartz adopt either the α- or β-quartz structure. As the stable polymorph of silica at room temperature, α-quartz (space group $P3_121$ or $P3_221$) transforms to the more expanded α-quartz (space group $P6_422$ or $P6_222$) at 846 K via the rotation of rigid tetrahedra about the *a* axes (Wright and Lehmann 1981; Will et al. 1988; Heaney 1994). Although pure β-quartz is not quenchable, the incorporation of small cations into its structural channels can prop open the framework and stabilize the β-quartz structure at room temperature. For example, the so-called LAS (Li_2O–Al_2O_3–SiO_2) phases with compositions $Li_{1-x}Al_{1-x}Si_{1+x}O_4$, $0 \le x < \sim 0.65$, possess the β-quartz structure. Like β-quartz, these phases exhibit negative coefficients of thermal expansion (CTE) (Pillars and Peacor 1973; Lichtenstein et al. 1998, 2000; Xu et al. 1999c, 2001a). As a result, they have served as major components of high-temperature glass–ceramic products used in domestic cookware and in many high-precision machines such as jet engines (Beall 1994; Müller 1995; Roy 1995; Ramalingam and Reimanis 2012). However, when the content of incorporated Li^+ falls below a certain threshold, i.e., $\sim 0.65 < x \le$

✉ Hongwu Xu
hxu@lanl.gov

[1] Earth and Environmental Sciences Division, Los Alamos National Laboratory, Los Alamos, NM 87545, USA

[2] Department of Geosciences, Pennsylvania State University, University Park, PA 16802, USA

[3] X-ray Science Division, Argonne National Laboratory, Argonne, IL 60439, USA

1 in $Li_{1-x}Al_{1-x}Si_{1+x}O_4$, the LAS phases adopt the α-quartz structure and possess positive CTEs. Furthermore, these α-quartz-like phases transform to their β-quartz-like counterparts at higher temperatures, and the transition temperature scales inversely with the Li content (Xu et al. 2001a).

To tailor the thermal properties of LAS phases for specific applications, other small cations, mainly Mg^{2+} and Zn^{2+}, have been used to partially replace Li^+ (Petzoldt 1967; Beall 1994). Whereas $Zn_{0.5-0.5x}Al_{1-x}Si_{1+x}O_4$, such as β-quartz and $Li_{1-x}Al_{1-x}Si_{1+x}O_4$ ($x < \sim 0.65$), exhibits negative CTEs, $Mg_{0.5-0.5x}Al_{1-x}Si_{1+x}O_4$ exhibits positive CTEs (Schreyer and Schairer 1961; Müller et al. 1988; Sternitzke and Müller 1991). In our recent study (Xu et al. 2015), we grew a $Mg_{0.5}AlSiO_4$ phase from glass and determined its structure using synchrotron XRD, transmission electron microscopy (TEM) and ^{29}Si nuclear magnetic resonance (NMR) spectroscopy. Our results indicate that this phase possesses an α-quartz-like structure with Mg occupying octahedral channel sites, in contrast to the tetrahedral coordination of Li in the β-quartz-type framework for β-eucryptite, $LiAlSiO_4$.

The motivation of this work is to examine the high-temperature structural behavior of $Mg_{0.5}AlSiO_4$. Since this phase is structurally analogous to α-quartz, will it undergo an α-to-β transformation on heating? How does the framework structure evolve as a function of temperature? What is the role of extra-framework Mg^{2+}? To answer these questions, we collected high-energy synchrotron XRD data of powdered $Mg_{0.5}AlSiO_4$ from 299 K to 1273 K and high-resolution synchrotron XRD data at 523 K and 748 K. Rietveld analysis indicates that $Mg_{0.5}AlSiO_4$ maintains its α-quartz-like structure throughout this temperature range. As in α-quartz, unit-cell dimensions increase with increasing temperature. However, the rates of increase are significantly smaller than those for α-quartz. This behavior can be attributed to the occupancy of Mg^{2+} over the octahedral channel sites, effectively hindering the [(Al,Si)O_4] tetrahedral tilting, which is the structural mechanism for thermal expansion of α-quartz-type framework and its transformation to the β-quartz-type configuration (Megaw 1973).

Experimental methods

$Mg_{0.5}AlSiO_4$ sample

The $Mg_{0.5}AlSiO_4$ sample was synthesized from heat-treatment of a glass of the same composition at 1173 K for ~ 7 h. Detailed synthesis procedures have been described in Xu et al. (2015). TEM observation and synchrotron XRD showed that the sample is homogeneous and phase pure. Energy-dispersive spectroscopy (EDS) analysis revealed that the chemical composition is essentially identical to the nominal $Mg_{0.5}AlSiO_4$ (Xu et al. 2015).

High-temperature synchrotron X-ray diffraction

We conducted two sets of powder synchrotron XRD experiments on $Mg_{0.5}AlSiO_4$ at high temperatures (Fig. 1). One set included high-resolution measurements at 523 K and 748 K with a linear position-sensitive detector at beam line X7A of the National Synchrotron Light Source (NSLS), Brookhaven National Laboratory (BNL) (Fig. 1a). The goal was to accurately determine the structure of $Mg_{0.5}AlSiO_4$ at high temperatures. The wavelength used was 0.700789 Å (17.7 keV in energy), as calibrated with a CeO_2 standard. Sample powders were sealed in a quartz-glass capillary of 0.02-mm diameter, which was mounted in a furnace consisting of a 1.25 inch-diameter wire-wound BN tube and outer water-cooled Al tube. Sample temperatures were registered with a Chromel–Alumel thermocouple positioned just below the center of the capillary, and was found to be stable within 1 K. To minimize preferred orientation, the capillary was fully rotated during data collection. Data were collected from 7° to 56° 2θ in the step-scan mode using step sizes of 0.25° and counting

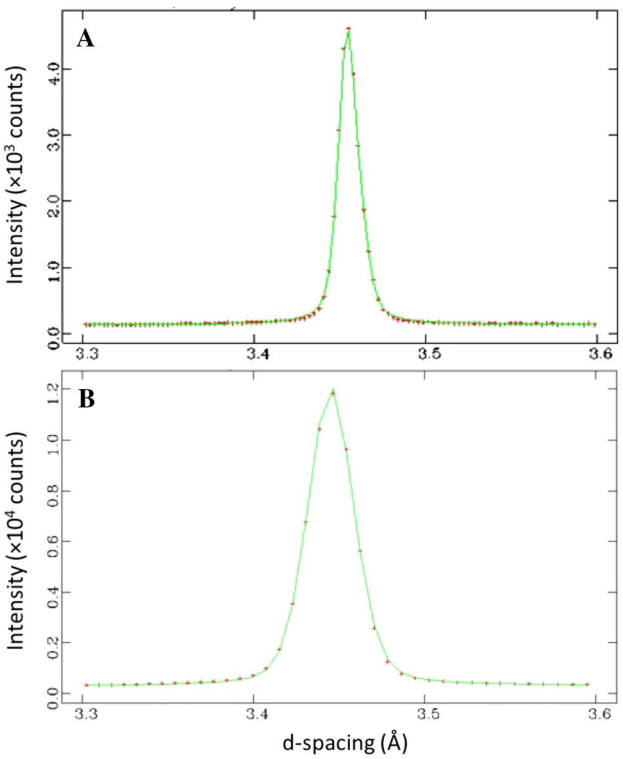

Fig. 1 Comparison of the strongest XRD peaks, (101), of $Mg_{0.5}AlSiO_4$ from room-temperature synchrotron data collected at **a** NSLS (Xu et al. 2015) and **b** APS. The NSLS data offer higher resolution (narrower peaks), whereas the APS data have superior counting statistics (compare the intensity scales). The slight difference in the (101) peak positions of the two patterns reflects systematic errors in the two diffractometers that were corrected during data processing

times of 10 s (7–15°), 20 s (15–30°), 40 s (30–45°), and 80 s (45–56°) per step.

Another set of XRD experiments included high-energy synchrotron measurements performed in a transmission mode at beam line 11-ID-C of the advanced photon source (APS), Argonne National Laboratory (ANL), taking advantage of quick data collection using high-energy synchrotron X-rays (Fig. 1b). The goal was to collect more XRD data at closely spaced temperature points within a larger range to gauge the critical temperature of the possible α–β transition in $Mg_{0.5}AlSiO_4$. The wavelength used was 0.11798 Å (105.1 keV in energy), as calibrated with a CeO_2 standard. Sample powders were packed into the chamber (8 mm in diameter and 3 mm deep) of a Linkam high-temperature furnace TS1500, and two-dimensional (2D) XRD patterns were collected continuously using a PerkinElmer large area detector when the sample was heated from room temperature to 1273 K with a heating rate of 10 K/min. A total of 747 data points were obtained. The 2D patterns were calibrated and converted to the conventional patterns of intensity versus 2θ using the Fit2d software. Selected temperature-dependent XRD patterns are shown in Fig. 2. Details of the experimental setup and data treatment can be found in Chen et al. (2011).

Rietveld analysis of XRD data

The above NSLS and APS synchrotron XRD data were analyzed by the Rietveld method with the general structure analysis system (GSAS) program (Larson and Von Dreele 2000) and GSAS-II (Toby and Von Dreele 2013), respectively. The starting structural parameters were taken from our previous study of the same sample at room temperature (Xu et al. 2015). Our refinements proceeded as follows: after the scale factor and four Chebyshev polynomial background terms had converged, specimen displacement and lattice parameters were added and optimized. Twelve (for the NSLS data) or eight (for the APS data) additional background terms were then added, and the peak profiles were fitted by refining isotropic and anisotropic broadening parameters and a Gaussian particle size coefficient in a pseudo-Voigt function (Thompson et al. 1987; Cox et al. 1988; Finger et al. 1994). On convergence of the preceding parameters, atomic positions and isotropic temperature factors for Mg, Al/Si, and O were refined.

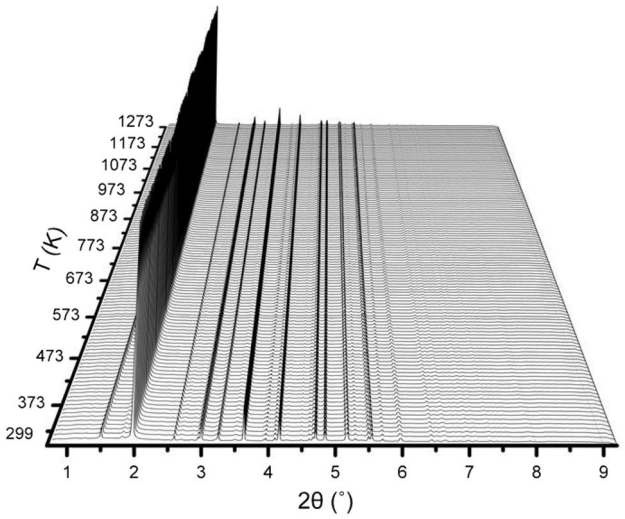

Fig. 2 Synchrotron XRD patterns of $Mg_{0.5}AlSiO_4$ at selected temperatures from room temperature to 1273 K. There is no obvious change among the patterns, consistent with the absence of a phase transformation in $Mg_{0.5}AlSiO_4$ on heating

Results and discussion

Framework structure

Xu et al. (2015) studied the structure of $Mg_{0.5}AlSiO_4$ using a combined approach of synchrotron XRD, electron diffraction and ^{29}Si NMR spectroscopy. The results indicate that the aluminosilicate framework adopts the structure of α-quartz with Al and Si being disordered over the tetrahedral sites at long-range scales (i.e., no doubled periodicity along the *c* axis, as would be expected due to Al/Si ordering in accordance with the so-called "Al avoidance" principle (Loewenstein 1954); though they are partially ordered at short-range scales, revealed by NMR). Mg exhibits different site occupancies within the neighboring channels parallel to the *c* axis, resulting in doubled periodicities along *a* relative to that of α-quartz. Thus the final refined structure was based on an *a*-doubled α-quartz-like superstructure (Xu et al. 2015). We analyzed the high-resolution high-temperature XRD data collected at NSLS using this superstructure model, and the refined structural parameters at 523 K and 748 K are listed in Tables 1 and 2, respectively. The corresponding fitted XRD patterns are plotted in Fig. 3a (for 523 K, refinement agreement indices $R_{wp}=4.4\%$, $\chi^2=2.37$) and 3B (for 748 K, $R_{wp}=5.1\%$, $\chi^2=2.06$). The analyses indicate that at high temperature, the aluminosilicate framework of $Mg_{0.5}AlSiO_4$ remains isostructural with α-quartz. Moreover, difference electron Fourier maps reveal that Mg occupies octahedral channel sites along the *c* axis (Fig. 4), as was observed at room temperature (Xu et al. 2015), and thus the site occupancies of Mg were fixed for all the temperatures in our refinements.

Nevertheless, for ease of describing structural variations in the α-quartz-like framework with temperature, especially with respect to the β-quartz-like configuration, one may neglect the superstructure and use the basic quartz unit cell to represent the $Mg_{0.5}AlSiO_4$ framework. In fact, the

Table 1 Unit-cell parameters, atomic coordinates and thermal parameters of $Mg_{0.5}AlSiO_4$ in the α-quartz superstructure model with doubled *a* axes (space group $P3_221$) at 523 K

Atom[a]	*x*	*y*	*z*	*U*iso[b]
Mg1	− 0.017(7)	0	1/6	4.6(5)
Mg2	0.495(8)	0	1/6	4.6(5)
Mg3	0.492(5)	0.510(6)	0.118(5)	4.6(5)
T1	0.256(2)	0	2/3	1.94(3)
T2	0.756(1)	0	2/3	1.94(3)
T3	0.255(1)	0.499(1)	0.664(2)	1.94(3)
O1	0.192(2)	0.111(2)	0.773(3)	3.7(1)
O2	0.691(2)	0.082(2)	0.854(3)	3.7(1)
O3	0.219(2)	0.614(3)	0.808(5)	3.7(1)
O4	0.712(2)	0.612(3)	0.801(5)	3.7(1)

Unit-cell parameters: $a = 10.4622(2)$ Å; $c = 5.3314(1)$ Å

[a]The occupancy of Mg1, Mg2 and Mg3 is ¼; T = Al, Si

[b]The unit of U_{iso} is Å/100; the U_{iso} values of like atoms are constrained to be equal

Table 2 Unit-cell parameters, atomic coordinates and thermal parameters of $Mg_{0.5}AlSiO_4$ in the α-quartz superstructure model with doubled *a* axes (space group $P3_221$) at 748 K

Atom[a]	*x*	*y*	*z*	U^b_{iso}
Mg1	− 0.011(9)	0	1/6	5.4(5)
Mg2	0.490(9)	0	1/6	5.4(5)
Mg3	0.492(6)	0.504(7)	0.108(5)	5.4(5)
T1	0.260(2)	0	2/3	2.43(5)
T2	0.754(2)	0	2/3	2.43(5)
T3	0.255(2)	0.499(2)	0.664(2)	2.43(5)
O1	0.193(3)	0.110(2)	0.771(3)	5.0(2)
O2	0.695(3)	0.092(3)	0.832(6)	5.0(2)
O3	0.202(4)	0.597(4)	0.834(5)	5.0(2)
O4	0.726(2)	0.622(3)	0.810(5)	5.0(2)

Unit-cell parameters: $a = 10.4782(2)$ Å; $c = 5.3378(2)$ Å

[a]The occupancy of Mg1, Mg2 and Mg3 is ¼; T = Al, Si

[b]The unit of U_{iso} is Å/100; the U_{iso} values of like atoms are constrained to be equal

superlattice peaks corresponding to the *a*-doubled periodicities are hardly visible in synchrotron XRD patterns, especially those collected at APS with moderate resolution (when the peaks are more diffuse) and at high temperatures (which may indicate possible disappearance of the superstructure at higher T). Hence, neglecting these weak, broad peaks in Rietveld analyses of XRD data does not induce significant errors in the refined $Mg_{0.5}AlSiO_4$ framework structure, and we used the average, basic α-quartz structure model to analyze all the high-temperature XRD data collected at APS, yielding refinement agreement indices of $R_{wp} = 4.6\%$ (1273 K)–6.8% (299 K) and $\chi^2 = 0.60$ (1273 K)–1.19 (299 K). The derived unit-cell parameters, atomic coordinates and atomic displacement parameters at a large number of closely spaced temperatures allow accurate characterization of framework variations in $Mg_{0.5}AlSiO_4$ as a function of temperature, as discussed below.

Thermal expansion

Figure 5 reveals the dependence of unit-cell parameters *a*, *c*, and unit-cell volume *V* of $Mg_{0.5}AlSiO_4$ on temperature. On heating, both *a* and *c* increase, and thus *V* also increases. To obtain the coefficients of thermal expansion (CTEs), we calculated a linear fit of the cell-parameter data as a function of temperature (*T*):

$$a = 3.178(2) \times 10^{-5} T + 5.20810(2) \quad R^2 = 0.9996, \qquad (1)$$

$$c = 2.456(4) \times 10^{-5} T + 5.31200(3) \quad R^2 = 0.9985, \qquad (2)$$

$$V = 2.119(2) \times 10^{-3} T + 124.772(2) \quad R^2 = 0.9994. \qquad (3)$$

The mean CTEs of $Mg_{0.5}AlSiO_4$ in the temperature range 299–1273 K are: $\alpha_a = 6.09(1) \times 10^{-6}$ K^{-1}; $\alpha_c = 4.62(2) \times 10^{-6}$ K^{-1}; and $\alpha_V = 1.690(4) \times 10^{-5}$ K^{-1}. These parameters are much lower than those of pure α-quartz, which first exhibits steady increases in *a*, *c* and *V* and then steep increases prior to its transformation to β-quartz at 846 K (Kihara 1990, 2001; Carpenter et al. 1998). For comparison, linear fittings of the *a*, *c* and *V* values of α-quartz in the temperature range 293–699 K (based on the XRD data of Carpenter et al. 1998) yield: $\alpha_a = 20(1) \times 10^{-6}$ K^{-1}; $\alpha_c = 13(1) \times 10^{-6}$ K^{-1}; and $\alpha_V = 5.2(4) \times 10^{-5}$ K^{-1}, which are about three times larger than the corresponding CTEs of $Mg_{0.5}AlSiO_4$. The CTEs of α-quartz in the temperature range prior to its transition to β-quartz (e.g., 700–846 K) are even larger, and they increase drastically as the temperature approaches the critical point, 846 K.

Mechanism of thermal expansion

As in α-quartz, the dominant mechanism responsible for the positive thermal expansion of $Mg_{0.5}AlSiO_4$ is a rotation of nearly rigid Si- or Al-tetrahedra around the *a* axes (in addition to the correlated changes in tetrahedral dimensions (Grimm and Dorner (1975)), which is associated with the low-frequency, high-amplitude phonon modes, most of which have negative Grüneisen coefficients (Xu and Heaney 1997; Smirnov 1999; Tucker et al. 2001). Figure 6 shows the temperature dependence of the tetrahedral rotation angle δ (Grimm and Dorner 1975)

$$\tan\delta = 2\sqrt{3}/9\,(c/a)\left[(1 - 6z)/x\right], \qquad (4).)$$

With increasing temperature, δ decreases gradually from ~ 9.4° at 299 K to ~ 7.1° at 1273 K. In other words, the

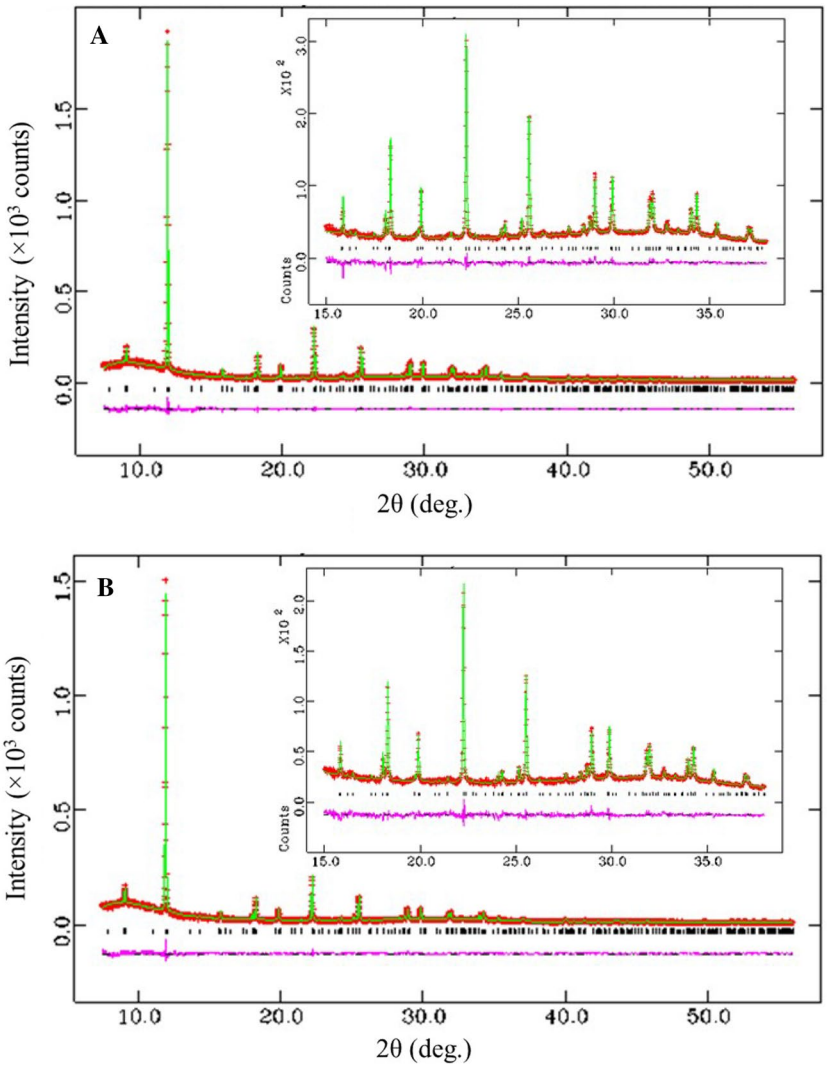

Fig. 3 Fitted synchrotron XRD patterns of $Mg_{0.5}AlSiO_4$ based on the α-quartz superstructure model with doubled *a* axes (space group $P3_221$) at **a** 523 K and **b** 748 K. Data are shown as plus signs, and the solid curve is the best fit to the data. Tick marks below the pattern show the positions of allowed reflections, and the lower curve represents the difference between the observed and calculated profiles. The inset shows the details of the profile from 15° to 38° 2*θ*

Al/Si-tetrahedral framework progresses towards the β-quartz configuration, where $\delta = 0$. However, even at the highest temperature tested (1273 K), δ does not reach zero, indicating that the framework structure remains in the α-quartz configuration. Extrapolation of the fitted δ–T linear relation:

$$\delta = 10.08(1) - 2.30(1) \times 10^{-3} T \quad R^2 = 0.9818, \tag{5}$$

to $\delta = 0$ yields a hypothetical α–β transition temperature of ~ 4383 K, which is well above the melting temperature (< 1573 K, Xu et al. 2015; Strnad 1986) of $Mg_{0.5}AlSiO_4$. By contrast, the rate of decrease in δ in α-quartz with increasing temperature is much larger; δ decreases from 15.8° at 298 K to 7.4° at 844 K, followed by a steep drop of 7.4° to reach $\delta = 0°$ in β-quartz from 844 to 847 K, a 3 K interval (Antao 2016). Temperature-dependent δ values have been fitted to an order parameter to describe the α–β quartz transition (Grimm and Dorner 1975; Carpenter et al. 1998).

The smaller rate of decrease in δ of $Mg_{0.5}AlSiO_4$ with increasing temperature and the absence of its β-quartz counterpart at high temperature can be attributed to the occupancy of the octahedral channel sites by Mg in $Mg_{0.5}AlSiO_4$. As shown in Fig. 7a, Mg^{2+} cations are situated at approximately the same *z* value as two O atoms in $[Si/AlO_4]$ tetrahedra from the two helical chains that spiral about *c*. On heating, the tetrahedra rotate about the *a* axes (Fig. 7b), as reflected by the decreases in δ. However, the presence of Mg in the octahedral channel sites hinders the tetrahedral tilting, resulting in a smaller rate of decrease in δ than occurs in α-quartz. The inhibitory effect of the channel Mg cations on tetrahedral tilting also explains the absence of a transition to a β-quartz-like $Mg_{0.5}AlSiO_4$ polymorph at high temperature.

It should be noted that the absence of an α–β transition at high temperature also occurs in other α-quartz-like phases with formula MXO_4 (e.g. $GaPO_4$), which have a M–O–X bridging angle of ≤ 136° or a rotational angle δ of ≥ 22° at room temperature. An inverse linear relation exists between M–O–X angle and δ, and the larger the

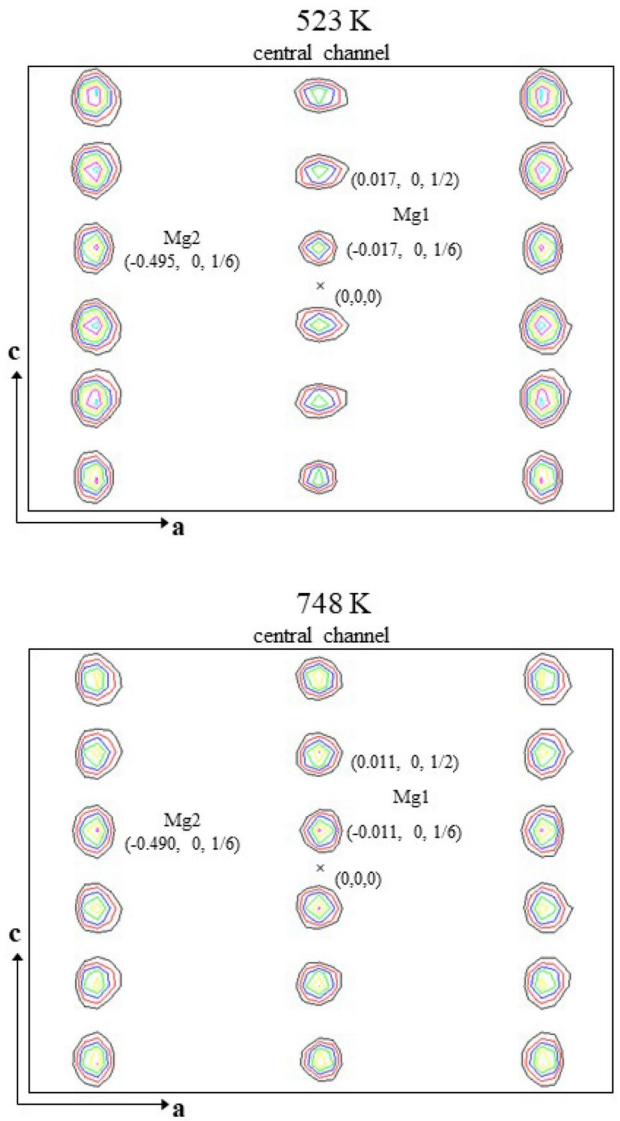

Fig. 4 Difference electron Fourier maps along the **a**–**c** plane of $Mg_{0.5}AlSiO_4$ showing the positions of Mg^{2+} in the structure channels at **A** 523 K and **B** 748 K. Contours are drawn from 0.9 to 2.7 $e^-/Å^3$ with an interval of 0.3 $e^-/Å^3$

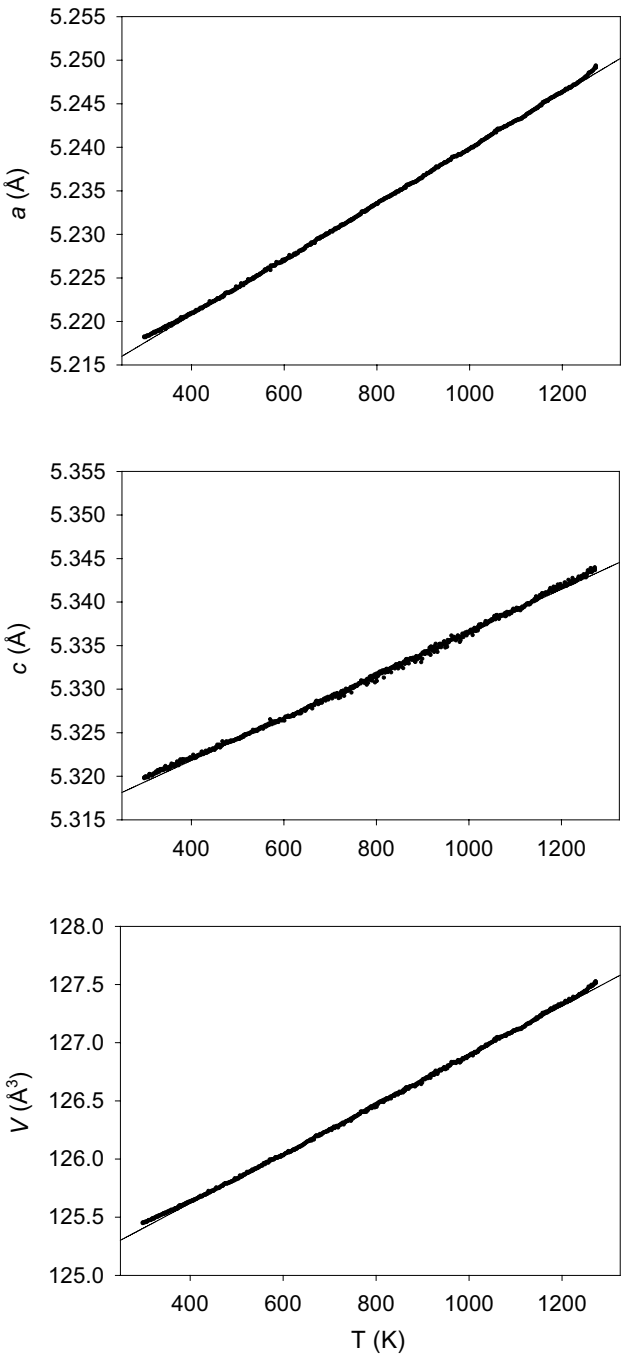

Fig. 5 Variation of **a** cell parameters a, **b** c, and **c** unit-cell volume V of $Mg_{0.5}AlSiO_4$ as a function of temperature. The lines are the best fit to the data

distortion of the tetrahedral chain, the smaller the M–O–X angle and the larger the value of δ (Philippot et al. 1994, 1996). However, the α-quartz-like $Mg_{0.5}AlSiO_4$ has an Al/Si–O–Al/Si angle of 148.4° and a rotational angle δ of ~ 9.4°. Therefore, the absence of the α–β transition in $Mg_{0.5}AlSiO_4$ is not due to its framework distortion (which is small). Rather, it results from the partial occupancy of Mg within the octahedral channel sites, hindering [Si/AlO_4] tetrahedral rotation about the a axes.

Variations of atomic displacement parameters with increasing temperature

Figure 8 shows variations in the isotropic displacement factors (U_{iso}) of Mg, Al/Si and O as a function of temperature. At a given temperature, $U_{iso}(O) > U_{iso}(Mg) > U_{iso}(Al/Si)$, which is consistent with the general trend that the lighter

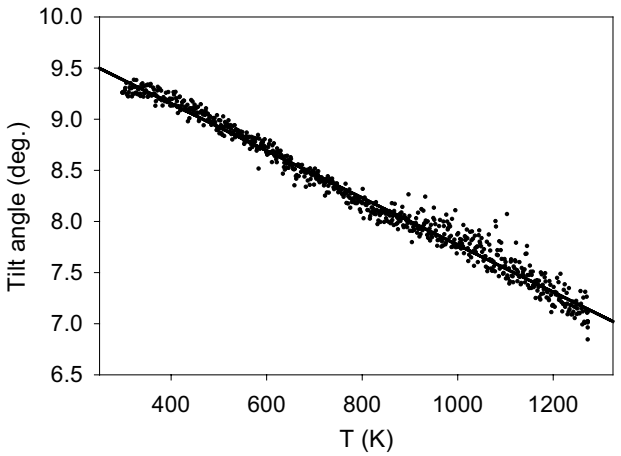

Fig. 6 Variation of the tilt angle for Al/Si-tetrahedra about the <100> axes in $Mg_{0.5}AlSiO_4$ as a function of temperature. The line is the best fit to the data

the element the larger the U_{iso}. For a given element, its U_{iso} increases with increasing temperature, as U ($=kT/f$, where k is the Boltzman constant, T is absolute temperature, and f is the bond force constant) is proportional to the temperature. However, the rate of increase of U_{iso}(Mg) on heating is much larger than those of U_{iso}(Al/Si) and U_{iso}(O) (The somewhat scattered U_{iso}(Mg) data points may be associated with the partial occupancy of Mg over the octahedral channel sites). This behavior may be explained in terms of the bonding configuration of Mg^{2+} with its neighboring atoms. In the α-quartz-like $Mg_{0.5}AlSiO_4$ structure, Mg is situated in the framework tunnels and thus has relatively weaker electrostatic interactions with its adjacent framework O, rendering greater vibrations with increasing temperature.

Effects of channel cation on structural variations of the quartz framework with temperature

The occupancy of the octahedral channel sites by Mg in $Mg_{0.5}AlSiO_4$ (Fig. 7a) is in striking contrast with that of the tetrahedral sites by Li in $LiAlSiO_4$. This disparity is responsible for not only the difference in the type of quartz-like framework at room temperature (α-quartz for $Mg_{0.5}AlSiO_4$ and β-quartz for $LiAlSiO_4$) but also its variations with temperature. Xu et al. (1999c) demonstrated that the β-quartz structure of $LiAlSiO_4$ persists down to low temperatures (20 K was the lowest temperature tested) without a β- to α-quartz-like transformation. Although Li positionally disorders within the structural channels along c at high temperature (Xu et al. 1999c; Zhang et al. 2003), the framework configuration does not experience a symmetry-breaking distortion in response to the order–disorder behavior of the Li^+ cations. In other words, the incorporation of Li into the quartz framework props open the β-quartz chain

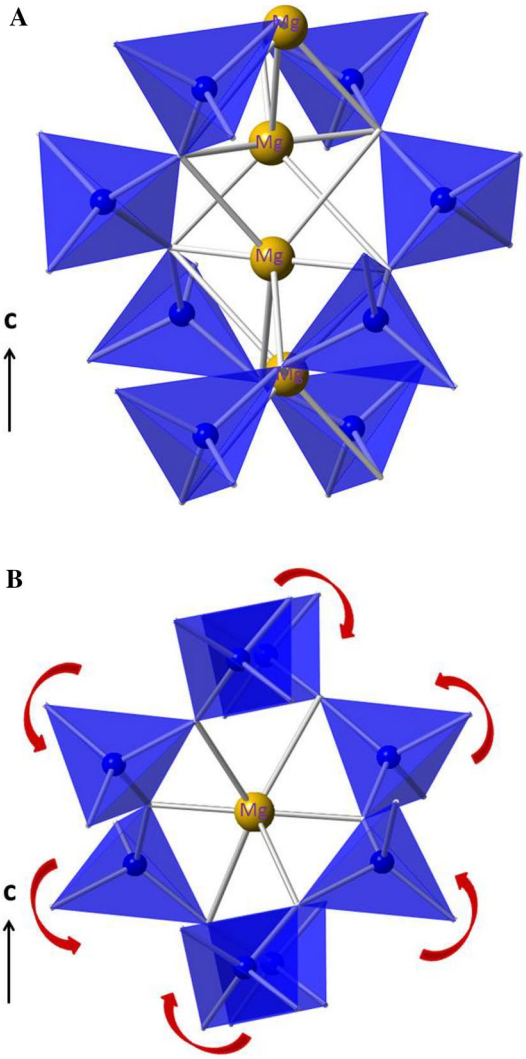

Fig. 7 **a** Coordination environments of Mg^{2+} in the α-quartz framework of $Mg_{0.5}AlSiO_4$. Tetrahedra represent [Si/AlO_4] units, and spheres represent Mg^{2+} cations. **b** Structure of $Mg_{0.5}AlSiO_4$ projected along [100], showing the rotation mechanism of [Si/AlO_4] tetrahedral around <100> axes on heating

configuration throughout the temperature range from 20 K (and likely from 0 K) to the melting point of $LiAlSiO_4$. As a result, $LiAlSiO_4$ exhibits negative thermal expansion in unit-cell volume, as in β-quartz, with its cell parameter c decreasing as a increases with increasing temperature. Likewise, the absence of the α- to β-quartz-like transition in $Mg_{0.5}AlSiO_4$ at high temperature implies that the α-quartz structure of $Mg_{0.5}AlSiO_4$ likely persists from 0 K to its melting point as well. Since the α-quartz configuration is the low-temperature polymorph, no transition is expected in $Mg_{0.5}AlSiO_4$ upon cooling. Moreover, as Mg is localized within the available octahedral channel sites (Figs. 4 and 7a), there is no order–disorder transition within a given channel parallel to c upon heating, as occurred with Li in $LiAlSiO_4$.

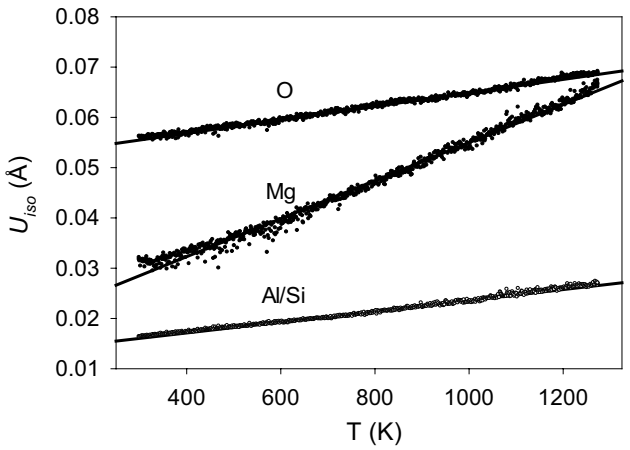

Fig. 8 Variation of isotropic thermal parameters (U_{iso}) for Mg, Al/Si and O in $Mg_{0.5}AlSiO_4$ as a function of temperature. The line is the best fit to the data

Correspondingly, the thermal expansion coefficients of $Mg_{0.5}AlSiO_4$ are positive along both the *a* and *c* axes, as in α-quartz, though the magnitudes are smaller. Therefore, the occupancy of Li^+ and Mg^{2+} over different channel sites in the quartz framework results in different polymorphs not only at room temperature but also above and below it.

Conclusions/implications

Silicate phases with framework structures commonly occur in natural rocks (e.g., feldspars) and in synthetic ceramic/composite materials (e.g., glass–ceramic cookware). Extra-framework cations situated in channels and/or cavities may exert significant effects on framework topologies (Xu et al. 2000b; Balmer et al. 2001), to the point of inducing symmetry changes at ambient conditions (Heaney 2000; Xu et al. 2001b, 2002). This phenomenon in turn affects the structural behaviors of doped phases upon changing temperature or pressure (Zhang et al. 2002, 2005; Chen et al. 2016). This study demonstrates the different responses of the quartz framework to the occupancy of Mg^{2+} and Li^+ within the channel sites. The presence of Mg^{2+} within the octahedral channel site stabilizes the α-quartz-like $Mg_{0.5}AlSiO_4$ structure up to its melting point, whereas the occupancy of Li^+ over the tetrahedral channel site maintains the β-quartz-like $LiAlSiO_4$ structure throughout the temperature range. Since the α- and β-quartz structures possess dramatically different thermal expansion properties (positive and negative thermal expansion for α- and β-quartz, respectively), one may design mixed Li/Mg-stuffed-quartz derivatives with tailored expansion properties (particularly zero thermal expansion). This information also has implications for the thermal behaviors of "impure" quartz and other framework aluminosilicate minerals during the formation of their host rocks.

Acknowledgements We thank J. L. Baker for plotting Fig. 2 and the two anonymous reviewers for helpful comments. This work was supported by the Laboratory Directed Research and Development (LDRD) program of Los Alamos National Laboratory (LANL). This research used resources of the Advanced Photon Source, a U.S. Department of Energy (DOE) Office of Science User Facility operated for the DOE Office of Science by Argonne National Laboratory under contract No. DE-AC02-06CH11357. Some experiments were carried out at the National Synchrotron Light Source, Brookhaven National Laboratory, which was supported by the U.S. Department of Energy, Office of Science, Office of Basic Energy Sciences, under contract No. DE-AC02-98CH10886. LANL, an affirmative action/equal opportunity employer, is managed by Triad National Security, LLC, for the National Nuclear Security Administration of the U.S. Department of Energy under contract 89233218CNA000001.

References

Antao SM (2016) Quartz: structural and thermodynamic analyses across the α ↔ β transition with origin of negative thermal expansion (NTE) in β quartz and calcite. Acta Cryst B72:249–262

Balmer ML, Su Y, Xu H, Bitten E, McCready D, Navrotsky A (2001) Synthesis, structure determination, and aqueous durability of $Cs_2ZrSi_3O_9$. J Am Ceram Soc 84:153–160

Beall GH (1994) Industrial applications of silica. Mineral Soc Am Rev Mineral 29:468–505

Buerger MJ (1954) The stuffed derivatives of the silica structures. Am Miner 39:600–614

Carpenter MA, Salje EKH, Graeme-Barber A, Wruck B, Dove MT, Knight KS (1998) Calibration of excess thermodynamic properties and elastic constant variations due to the α-β phase transition in quartz. Am Miner 83:2–22

Chen Z, Qin Y, Ren Y, Lu W, Orendorff C, Roth EP, Amine K (2011) Multi-scale study of thermal stability of lithiated graphite. Energy Environ Sci 4:4023–4030

Chen Y, Manna S, Narayanan B, Wang Z, Reimanis IE, Ciobanu CV (2016) Pressure-induced phase transformation in β-eucryptite: an X-ray diffraction and density functional theory study. Scripta Mater 122:64–67

Cox DE, Toby BH, Eddy MM (1988) Acquisition of powder diffraction data with synchrotron radiation. Aust J Phys 41:117–131

Finger LW, Cox DE, Jephcoat AP (1994) A correction for powder diffraction peak asymmetry due to axial divergence. J Appl Crystallogr 27:892–900

Ghiorso MS, Carmichael ISE, Moret LK (1979) Inverted high-temperature quartz. Contrib Miner Petrol 68:307–323

Grimm H, Dorner B (1975) On the mechanism of the α-β phase transformation of quartz. J Phys Chem Solids 36:407–413

Guth H, Heger G (1979) Temperature dependence of the crystal structure of the one-dimensional Li^+-conductor β-eucryptite ($LiAlSiO_4$). In: Vashista P, Mundy JN, Shenoy GK (eds) Fast ion transport in solids. Elsevier North Holland, New York, pp 499–502

Heaney PJ (1994) Structure and chemistry of the low-pressure silica polymorphs. Mineral Soc Am Rev Mineral Geochem 29:1–40

Heaney PJ (2000) Phase transformations induced by solid solution. Mineral Soc Am Rev Mineral Geochem 39:135–174

Keith ML, Tuttle OF (1952) Significance of variance in high-low inversion of quartz. Am J Sci 253a:203–280

Kihara K (1990) An X-ray study of the temperature dependence of the quartz structure. Eur J Mineral 2:63–77
Kihara K (2001) Molecular dynamics interpretation of structural changes in quartz. Phys Chem Miner 28:365–376
Larson AC, Von Dreele RB (2000) GSAS–general structure analysis system. Los Alamos National Laboratory Report No. LAUR 86-748, p 179
Lichtenstein AI, Jones RO, Xu H, Heaney PJ (1998) Anisotropic thermal expansion in the silicate β-eucryptite: a neutron diffraction and density functional study. Phys Rev B 58:6219–6223
Lichtenstein AI, Jones RO, de Gironcoli S, Baroni S (2000) Anisotropic thermal expansion in silicates: a density functional study of β-eucryptite and related materials. Phys Rev B 62:11487–11493
Loewenstein W (1954) The distribution of aluminum in the tetrahedra of silicates and aluminates. Am Miner 39:92–96
Megaw H (1973) Crystal structures: a working approach. WB Saunders, Philadelphia
Müller G (1995) The scientific basis. In: Bach H (ed) Low thermal expansion glass ceramics. Springer-Verlag, Berlin, pp 13–49
Müller G, Hoffmann M, Neeff R (1988) Hydrogen substitution in lithium-aluminosilicates. J Mater Sci 23:1779–1785
Müller G, Paulus H, Darmstadt JS (1990) Synthesis and structure of β-quartz type Na0.5H0.5AlSi2O6 as compared to LiAlSi2O6. N Jb Miner Mh H11:493–503
Palmer DC (1994) Stuffed derivatives of the silica polymorphs. Mineral Soc Am Rev Mineral 29:83–122
Paulus H, Fuess H, Müller G, Darmstadt JS, Vogt T (1990) The crystal structure of β-quartz type HAlSi2O6. N Jb Miner Mh H5:232–240
Petzoldt J (1967) Metastabile mischkristalle mit quarzstruktur mit oxidsystem Li_2O-MgO-ZnO-Al_2O_3-SiO_2. Glastechnische Berichte 40:385–396
Philippot E, Goiffon A, Ibanez A, Pintard M (1994) Structure deformations and existence of the α-β transition in MXO_4 quartz-like materials. J Solid State Chem 110:356–362
Philippot E, Palmier D, Pintard M, Goiffon A (1996) A general survey of quartz and quartz-like materials: packing distortions, temperature, and pressure effects. J Solid State Chem 123:1–13
Phillips BL, Xu H, Heaney PJ, Navrotsky A (2000) 29Si and 27Al MAS-NMR spectroscopy of β-eucryptite (LiAlSiO4): the enthalpy of Si, Al ordering. Am Miner 85:181–188
Pillars WW, Peacor DR (1973) The crystal structure of beta eucryptite as a function of temperature. Am Miner 58:681–690
Ramalingam S, Reimanis IE (2012) Effect of doping on the thermal expansion of β-eucryptite prepared by sol-gel methods. J Am Ceram Soc 95:2939–2943
Roy R (1995) Low thermal expansion ceramics: A retrospective. In: Stinton DP, Limaye SY (eds) Low-expansion materials, ceramic transactions, vol 52. The American Ceramic Society. Westerville, Ohio, USA, pp 1–4
Schreyer W, Schairer JF (1961) Metastable solid solution with quartz-type structure on the join SiO_2-$MgAl_2O_4$. Z Kristallogr 116:60–82
Schulz H (1971) Influence of heat-treatment on the average structure of $Mg[Al_2Si_3O_{10}]$, a stuffed derivative of the high-quartz structure. Zeitschrift für Kristallographie Bd 134:253–261
Schulz H, Muchow GM, Hoffmann W, Bayer G (1971a) X-ray study of Mg-Al silicate high-quartz phases. Zeitschrift für Kristallographie Bd 133:91–109
Schulz H, Hoffmann W, Muchow GM (1971b) The average structure of $Mg[Al_2Si_3O_{10}]$, a stuffed derivative of the high-quartz structure. Zeitschrift für Kristallographie Bd 134:1–27
Smirnov MB (1999) Lattice dynamics and thermal expansion of quartz. Phys Rev B 59:4036–4043
Smith JV, Steele IM (1984) Chemical substitution in silica polymorphs. Neues Jahrbuch für Mineralogie Monatschefte 3:137–144
Sternitzke M, Müller G (1991) Crystal structure and thermal expansion of quartz-type aluminosilicates. J Mater Sci 26:3051–3056
Strnad Z (1986) Glass-ceramic materials. Glass science and technology, vol 8. Elsevier, Amsterdam, p 268
Thompson P, Cox DE, Hastings J (1987) Rietveld refinement of Debye-Scherrer synchrotron X-ray data for Al_2O_3. J Appl Crystallogr 20:79–83
Toby BH, Von Dreele RB (2013) GSAS-II: the genesis of a modern open-source all purpose crystallography software package. J Appl Crystallogr 46:544–549
Tscherry V, Schulz H, Laves F (1972) Average and super structure of β-eucryptite ($LiAlSiO_4$), part II, superstructure. Z Kristallogr 135:175–198
Tucker MG, Keen DA, Dove MT (2001) A detailed structural characterization of quartz on heating through the α–β phase transition. Mineral Mag 65:489–507
Will G, Bellotto M, Parrish W, Hart M (1988) Crystal structures of quartz and magnesium germanate by profile analysis of powder diffractometer data. J Appl Crystallogr 21:182–191
Wright AF, Lehmann MS (1981) The structure of quartz at 25 and 500°C determined by neutron diffraction. J Solid State Chem 36:371–380
Xu H, Heaney PJ (1997) Memory effects of domain structures during displacive phase transitions: a high-temperature TEM study of quartz and anorthite. Am Miner 82:99–108
Xu H, Heaney PJ, Navrotsky A, Topor L, Liu J (1999a) Thermochemistry of stuffed quartz-derivative phases along the join $LiAlSiO_4$-SiO_2. Am Miner 84:1360–1369
Xu H, Heaney PJ, Böhm H (1999b) Structural modulations and phase transitions in β-eucryptite: an in situ TEM study. Phys Chem Miner 26:633–643
Xu H, Heaney PJ, Yates DM, Von Dreele RB, Bourke MA (1999c) Structural mechanisms underlying near-zero thermal expansion in β-eucryptite: a combined synchrotron X-ray and neutron Rietveld analysis. J Mater Res 14:3138–3151
Xu H, Heaney PJ, Beall GH (2000a) Phase transitions induced by solid solution in stuffed derivatives of quartz: a powder synchrotron XRD study of the $LiAlSiO_4$-SiO_2 join. Am Miner 85:971–979
Xu H, Navrotsky A, Nyman MD, Nenoff TM (2000b) Thermochemistry of microporous silicotitanate phases in the Na_2O–Cs_2O–SiO_2–TiO_2–H_2O system. J Mater Res 15:815–823
Xu H, Heaney PJ, Navrotsky A (2001a) Thermal expansion and structural transformations of stuffed derivatives of quartz along the $LiAlSiO_4$-SiO_2 join: a variable-temperature powder synchrotron XRD study. Phys Chem Miner 28:302–312
Xu H, Navrotsky A, Balmer ML, Su Y, Bitten ER (2001b) Energetics of substituted pollucites along the CsAlSi2O6–CsTiSi2O6.5 join: a high-temperature calorimetric study. J Am Ceram Soc 84:555–560
Xu H, Navrotsky A, Balmer ML, Su Y (2002) Crystal chemistry and phase transitions in substituted pollucites along the CsAlSi2O6-CsTiSi2O6.5 join: a powder synchrotron X-ray diffractometry study. J Am Ceram Soc 85:1235–1242
Xu H, Heaney PJ, Yu P, Xu H (2015) Synthesis and structure of a stuffed derivative of α-quartz, $Mg_{0.5}AlSiO_4$. Am Miner 100:2191–2198
Zhang J, Celestian A, Parise JB, Xu H, Heaney PJ (2002) A new polymorph of eucryptite ($LiAlSiO_4$), ε-eucryptite, and thermal expansion of α- and ε-eucryptite at high pressure. Am Miner 87:566–571
Zhang M, Xu H, Salje EKH, Heaney PJ (2003) Vibrational spectroscopy of beta-eucryptite ($LiAlSiO_4$): optical phonons and phase transition(s). Phys Chem Miner 30:457–462
Zhang J, Zhao Y, Xu H, Zelinskas MV, Wang L, Wang Y, Uchida T (2005) Pressure-induced amorphization and phase transformations in β-$LiAlSiO_4$. Chem Mater 17:2817–2824